

# Geophysical Research Letters



## RESEARCH LETTER

10.1029/2021GL093466

### Key Points:

- The quasi-2-day waves (Q2DW) wind field at 80–200 km altitude is delineated from combining ground and space data in the low-latitude region (+/−15°)
- Zonal wavenumber components  $s = +2$  and  $s = +3$  are the dominant ones in our observations, and their wave periods evolve differently with time
- The quasi-2-day waves  $s = +3$  exhibits an excellent quantitative agreement between two datasets at 95–100 km, serving as a validation of the ICON-MIGHTI winds

### Supporting Information:

Supporting Information may be found in the online version of this article.

### Correspondence to:

J. L. Chau,  
[chau@iap-kborn.de](mailto:chau@iap-kborn.de)

### Citation:

He, M., Chau, J. L., Forbes, J. M., Zhang, X., Englert, C. R., Harding, B. J., et al. (2021). Quasi-2-day wave in low-latitude atmospheric winds as viewed from the ground and space during January–March, 2020. *Geophysical Research Letters*, 48, e2021GL093466. <https://doi.org/10.1029/2021GL093466>

Received 19 MAR 2021

Accepted 9 JUN 2021

© 2021. The Authors.

This is an open access article under the terms of the [Creative Commons Attribution-NonCommercial License](https://creativecommons.org/licenses/by-nc/4.0/), which permits use, distribution and reproduction in any medium, provided the original work is properly cited and is not used for commercial purposes.

## Quasi-2-Day Wave in Low-Latitude Atmospheric Winds as Viewed From the Ground and Space During January–March, 2020

Maosheng He<sup>1</sup> , Jorge L. Chau<sup>1</sup> , Jeffrey M. Forbes<sup>2</sup> , Xiaoli Zhang<sup>2</sup> , Christoph R. Englert<sup>3</sup> , Brian J. Harding<sup>4</sup> , Thomas J. Immel<sup>4</sup>, Lourivaldo M. Lima<sup>5</sup> , S. Vijaya Bhaskar Rao<sup>6</sup>, M. Venkat Ratnam<sup>7</sup> , Guozhu Li<sup>8,9</sup> , John M. Harlander<sup>10</sup> , Kenneth D. Marr<sup>3</sup>, and Jonathan J. Makela<sup>11</sup> 

<sup>1</sup>Leibniz-Institute of Atmospheric Physics at the University of Rostock University, Kühlungsborn, Germany,

<sup>2</sup>Ann & H.J. Smead Department of Aerospace Engineering Sciences, University of Colorado, Boulder, USA, <sup>3</sup>U.S.

Naval Research Laboratory, Washington, DC, USA, <sup>4</sup>Space Sciences Laboratory, University of California Berkeley,

Berkeley, CA, USA, <sup>5</sup>Universidade Estadual da Paraíba, Brazil, <sup>6</sup>Department of Physics, Sri Venkateswara University,

Tirupati, India, <sup>7</sup>National Atmospheric Research Laboratory, Tirupati, India, <sup>8</sup>Beijing National Observatory of Space

Environment, Institute of Geology and Geophysics, Chinese Academy of Sciences, Beijing, China, <sup>9</sup>College of Earth and

Planetary Sciences, University of Chinese Academy of Sciences, Beijing, China, <sup>10</sup>Space Systems Research Corporation,

Alexandria, VA, USA, <sup>11</sup>Department of Electrical and Computer Engineering, University of Illinois Urbana-Champaign,

Urbana, IL, USA

**Abstract** Horizontal winds from four low-latitude ( $\pm 15^\circ$ ) specular meteor radars (SMRs) and the Michelson Interferometer for Global High-resolution Thermospheric Imaging (MIGHTI) instrument on the ICON satellite, are combined to investigate quasi-2-day waves (Q2DWs) in early 2020. SMRs cover 80–100 km altitude whereas MIGHTI covers 95–300 km. Q2DWs are the largest dynamical feature of the summertime middle atmosphere. At the overlapping altitudes, comparisons between the derived Q2DWs exhibit excellent agreement. The SMR sensor array analyses show that the dominant zonal wavenumbers are  $s = +2$  and  $+3$ , and help resolve ambiguities in MIGHTI results. We present the first Q2DW depiction for  $s = +2$  and  $s = +3$  between 95 and 200 km, and show that their amplitudes are almost invariant between 80 and 100 km. Above 106 km, Q2DW amplitudes and phases present structures that might result from the superposition of Q2DWs and their aliased secondary waves.

**Plain Language Summary** In the mesosphere and lower-thermosphere, quasi-2-day waves are spectacular planetary-scale oscillations. Almost all relevant observational studies are based on ground-based single-station or single-satellite methods and therefore cannot determine the zonal wavenumber unambiguously. In the current work, we employ a series of multi-station methods on winds measured by four longitudinally separated low-latitude ground-based radars. These methods help us to determine two dominant zonal wavenumbers at 80–100 km altitude. These results are used to complement satellite measurements. The agreement between datasets is extraordinary, allowing us to extend the characteristics of the waves to higher altitudes using satellite measurements.

## 1. Introduction

Quasi-two-day waves (Q2DWs) in the mesosphere have been the subject of numerous observational and theoretical investigations (e.g., Pancheva et al., 2018, and references therein) since their first discovery in specular meteor radar (SMR) winds (Müller, 1972). Q2DWs are generally thought to be the atmospheric manifestation of the gravest westward-propagating Rossby-gravity normal mode with zonal wavenumber  $s = 3$  (Salby, 1981; Salby & Roper, 1980), amplified or perhaps even initiated by the mesospheric easterly jet instability (Plumb, 1983; Pfister, 1985; Randel, 1994), which admits zonal wavenumbers of  $s = 2$  through 4. Q2DWs with  $s = 2, 3$ , and 4 are common features of space-based observational studies (e.g., Gu et al., 2013; Huang et al., 2013; Lieberman, 1999; Tunbridge et al., 2011).

Being the largest dynamical feature of the summertime middle atmosphere, Q2DWs play a significant role in atmosphere-ionosphere coupling. Although earlier works have suggested that Q2DWs could drive

F-region ionospheric variability (Chen, 1992; Ito et al., 1986; Pancheva, 1988; Pancheva & Lysenko, 1988), it was not until the last decade that a general circulation model (GCM) including ionospheric electrodynamics demonstrated that the Q2DWs could penetrate above 100 km to produce dynamo electric fields that drive Q2DW ionospheric variability in the F-region (Yue, Wang et al., 2012). However, it is also known that such penetration is highly sensitive to the zonal-mean wind distribution above 100 km, which is poorly understood (Yue, Liu, & Chang, 2012). In addition, there are remaining questions concerning other ways in which Q2DWs transmit their influence to the ionosphere, including the modulation of tides (Yue et al., 2016) and gravity waves (Meyer, 1999). Other relevant aspects of the problem include the latitude and longitude structures of Q2DWs at any given time. Therefore, further study of the spatial-temporal evolution of Q2DWs and their interactions with other waves appears warranted before a complete understanding of atmosphere-ionosphere coupling is attained.

The pros and cons of ground- and space-based measurements of Q2DWs in the mesosphere and lower thermosphere (MLT) are well-known. Single-station ground-based measurements provide excellent temporal resolution but no information on their horizontal wavenumber (e.g., Harris & Vincent, 1993). On the other hand, satellite measurements provide a more global view in terms of spatial coverage, but suffer from crude temporal resolution and, most significantly, aliasing (Tunbridge et al., 2011; Forbes & Moudden, 2012; Nguyen et al., 2016). When viewed from a quasi-Sun-synchronous perspective in space, a wave at frequency  $f$  with zonal wavenumber  $s$  is Doppler-shifted such that its longitude structure appears at its “space-based zonal wavenumber”  $k_s = \left| s - \frac{f}{1\text{cpd}} \right|$ , where cpd is cycles per day (e.g., Forbes & Moudden, 2012).

Accordingly, the Q2DW+3 (hereafter, Q2DW $p$  denotes a Q2DW with wavenumber  $s = p$ ) appears at  $k_s = 2.5$ , and so do secondary waves (SWs) of nonlinear interactions between Q2DW+3 and all migrating tides (Forbes & Moudden, 2012; Nguyen et al., 2016; Tunbridge et al., 2011). These SWs are at frequencies near 0.5, 1.5, 2.5, 3.5, ..., cpd, namely, at periods near 2 days, 16 h, 9.6 h, 6.9 h,...(e.g., He et al., 2021). In other words, these waves will alias into each other when observed from quasi-Sun-synchronous single-spacecraft missions. Among these waves is the Q2DW-2, the near-2-days SW from a Q2DW+3 interaction with the migrating diurnal tide. Similarly, Q2DW+2 and Q2DW+4 can alias with Q2DW-1 and Q2DW-3 at  $k_s = 2.5$  and 3.5, respectively. Both Q2DW-2 and Q2DW-3 can arise from jet instabilities at middle to high latitudes during local winter (Pancheva et al., 2016), and all three eastward-propagating Q2DWs can coexist at low latitudes in the form of ultra-fast Kelvin waves (UFWK) (e.g., Forbes, He, et al., 2020; Pancheva et al., 2016).

Despite the importance of dynamo-region winds to Q2DW-ionosphere coupling, wind observations are extremely rare above about 105 km. One exception appears to be Ward et al. (1996) who reported Q2DW+3 winds between 90 and 150 km from Wind Imaging Interferometer (WINDII) daytime measurements on the Upper Atmosphere Research Satellite (UARS) during January 1993. Nighttime satellite measurements are unavailable above 105–110 km due to lack of airglow. This exacerbates sampling issues associated with space-based observations.

As suggested by Harris and Vincent (1993), combining more than one ground-based station with appropriate separation, could enable the determination of Q2DWs wavenumbers. In the present work, we combine horizontal winds from multiple SMRs (MSMR) located at four different longitudes at low latitudes, and from Michelson Interferometer for Global High-resolution Thermospheric Imaging (MIGHTI) on NASA’s ICON (Ionospheric CONnection explorer) satellite (Immel et al., 2018). This combination allows us to obtain a comprehensive view of the Q2DWs that occurred during January–March 2020. Combining the MSMR and MIGHTI analyses, we are able to characterize clearly the dominant Q2DWs in time, altitude, frequency, wavenumber, and latitude.

## 2. Data Analysis

The current work investigates Q2DWs using MLT zonal ( $u$ ) and meridional ( $v$ ) winds collected on the ground and from space. Ground-based winds were obtained between 80 and 100 km every hour at four SMRs: Peru (77°W, 12°S), and Cariri (36.5°W, 7.4°S), Tirupati (79.4°E, 13.6°N) and Ledong (109.0°E, 18.4°N). Characteristics and some results of each of these SMRs can be found in Chau et al. (2021), Lima et al. (2012), Rao et al. (2014), and Wang et al. (2019), respectively. The space-based winds are collected by the MIGHTI

instrument on ICON (Englert et al., 2017). From a theoretical study, MIGHTI's wind accuracy is better than  $5.8 \text{ ms}^{-1}$  80% of the time. The exceptions occur near the day/night boundaries and occasionally near the equatorial ionization anomaly (in the F-region), due to variations of wind and emission rate along the line-of-sight (Harding et al., 2017). Recently, MIGHTI winds in the F-region (red line) and E-region (green line) have been validated against Fabry-Perot interferometers and SMRs, respectively (Harding et al., 2021; Makela et al., 2021). At low latitudes, Q2DWs maximize annually between January and March (e.g., Harris & Vincent, 1993; Rao et al., 2017), thus, our study is focused on the January–March 2020 period.

### 2.1. Multi-Station Specular Meteor Radar Analyses

At a given frequency  $f$ , longitude  $\lambda$ , and time  $t$ , the superposition of zonal traveling waves, indexed as  $l = 1, 2, \dots, L$ , with zonal wavenumbers  $s_l$ , can be denoted as,

$$\sum_{l=1,2,\dots,L} \tilde{\Psi}(\lambda, t | f, s_l) = e^{i2\pi ft} \tilde{a}_\lambda \quad (1)$$

where  $\tilde{a}_\lambda = \sum \tilde{A}(\lambda | s_l)$  and  $\tilde{A}(\lambda | s_l) = \tilde{A}_l e^{is_l \lambda}$  is the longitude-dependent complex amplitude. We estimate  $\tilde{a}_\lambda$  as a function of  $f$ ,  $t$ , and altitude  $h$ , through Lomb-Scargle spectral analyses within a 23-days wide sliding window for each of the wind components of each SMR. The resultant  $\tilde{a}_\lambda(t, f, h)$  enable estimation of  $s$  and  $\tilde{A}_l$  using a variety of sensor array analyses.

Assuming a single dominant wave, that is,  $L = 1$ , one can apply the phase difference technique to a pair of SMRs (e.g., He et al., 2018). The single-wave assumption is often facilitated through high-frequency-resolved wavelet or Lomb-Scargle analyses by separating waves in the frequency domain (e.g., He et al., 2018). The current work applies this technique to Tirupati-Ledong and Peru-Cariri pairs, separately. These pairs have been selected given their similar latitudes with longitudinal separations far enough to resolve Q2DWs zonal wavenumbers.

The same wind data have also been analyzed, assuming a dominant wave (i.e.,  $L = 1$ ) weakly dependent in latitude. In this case, a least-square estimation (LSE) method similar to equation A3 in He et al. (2020) has been applied to the altitude-averaged Lomb-Scargle estimations  $\langle \tilde{a}_\lambda(t, f, h) \rangle$  from all four radars. This analysis allows determining the dominant wavenumbers for a given period and time.

As we will see later in Section 3, the two techniques implemented above reveal that the Q2DWs are dominated mainly by two wavenumbers. While both techniques use the single-wave assumption, these two dominant waves might superpose on each other. To decompose the potential superposition and estimate the wave amplitudes, we implement an LSE to Equation 1 after relaxing the single-wave assumption to a two-wave assumption, that is,  $L = 2$ . A similar procedure was applied by He and Chau (2019) but for near-12-h waves. In the results presented below, the amplitudes are set to zeros either when  $\langle \tilde{a}_\lambda(t, f, h) \rangle$  are below the significance level  $\alpha = 0.01$  at more than two stations or when the coefficient of determination of the LSE is below  $r^2 = 0.7$ . The significance level is estimated through a Monte Carlo method.

### 2.2. ICON-MIGHTI Winds

As a slowly precessing low-earth-orbit satellite, ICON orbits at 590–607 km altitude about 15 times per day. ICON crosses a given latitude once in the ascending or descending leg which covers all local solar times once every 46 days, namely, one orbital precession period. Constrained by the  $27^\circ$  orbital inclination and MIGHTI's viewing geometry off the north side of the spacecraft, the winds are derived between  $12^\circ\text{S}$  and  $42^\circ\text{N}$  latitude. The ascending-descending differences in the local time are latitude-dependent, which increases from near zero at  $12^\circ\text{S}$  to almost 12 h near  $18^\circ\text{N}$  and then decreases to less than 2 h at  $42^\circ\text{N}$ . MIGHTI winds are derived from the Doppler shift of airglow emissions along with two perpendicular tangent-point line-of-sight vector measurements on the limb. Due to the day-night difference of the airglow's vertical distribution, the altitude coverage of the observations is different between day and night. While the nighttime wind is derived from about 94–106 km, the daytime wind is available at least up to 300 km. In this work, we use the green-line winds flagged as “good” and “caution,” that is, with quality flags 1.0 and 0.5, respectively

(e.g., Harding et al., 2021). Absolute wind amplitudes above three times the median value are considered outliers.

At 96–106 km altitude, we estimate Q2DW amplitudes as a function of time, frequency, latitude and altitude, by fitting data sampled within a 23 days sliding window, irrespective of the local time, to a single wave model  $\tilde{A}_0(s)e^{i(2\pi ft+s\lambda)}$ , for  $s = 2$  and  $3$ , respectively. Above 106 km and for the amplitude fitting, we sample the daytime only data within time intervals when strong Q2DWs are detected below 106 km, for example, day of the year (DOY) 15–23 and DOY 39–46. As an example of the data distribution within these two intervals, Figure S1 in the supplemental information presents the samplings as a function of time and subdivided longitude (cf., Moudden & Forbes, 2014) at a given latitude and altitude.

### 3. Results

Under the single-wave assumption, dominant wavenumbers were obtained by (a) using the phase difference technique on SMR pairs, and (b) using LSE on all four SMRs but assuming a weak latitudinal dependence. We found that in both cases the dominant Q2DW wavenumbers were  $s = 3$  and  $s = 2$ , that is, Q2DW+3, and Q2DW+2, respectively. Climatologically, these two Q2DWs are also dominant in the southern hemisphere (see Tunbridge et al., 2011, Figure 7). Furthermore, we find that the meridional component is much stronger than the zonal component for both dominant wavenumbers. The results of these two analyses are presented in the supporting information Figures S2 and S3, respectively.

Based on these supporting results, we present the results of relaxing the assumption of one dominant wave-number for a given time, frequency and altitude, to allow two, that is,  $L = 2$ . Figure 1 shows the meridional amplitudes as a function of time and period resulting from fitting for  $s = 2$  (left) and  $s = 3$  (right) at four altitude ranges, that is, 80–85 km, 85–90 km, 90–95 km, and 95–100 km.

As displayed in Figures 1a and 1b, the Q2DW+2 (Q2DW+3) amplitude at 95–100 km altitude maximizes within DOY 40–75 (10–40) at period 44–48 (48–53) h for amplitudes above  $15 \text{ ms}^{-1}$  ( $30 \text{ ms}^{-1}$ ). The period and amplitude variations of Q2DW+2 and Q2DW+3 at 95–100 km altitude are similar to those at the other three altitudes.

MIGHTI winds complement the MSMR results by extending the Q2DW amplitudes to broader latitude and altitude ranges. In the time-latitude structures of the MIGHTI Q2DWs at 98 km, as shown in Figure 2, the meridional wind ( $v$ ) amplitudes of both Q2DWs are significantly stronger than the zonal wind ( $u$ ) amplitudes, consistent with MSMR results in Figure S2. In  $v$ , both Q2DWs attain values of order  $20\text{--}30 \text{ ms}^{-1}$  within  $\pm 12^\circ$  latitude and maximize around the equator. The  $u$  amplitudes attain values above  $10 \text{ ms}^{-1}$  which is confined to latitudes poleward of  $10^\circ\text{N}$ .

In Figure 3 we present a qualitative and quantitative comparison of the estimated Q2DW amplitudes obtained with MSMR and MIGHTI. In Figures 3a–3d, the time-frequency spectra of the MSMR Q2DW amplitudes at 95–100 km are in good qualitative agreement with MIGHTI estimates at 98 km. For a quantitative comparison, we sample every pixel in the MIGHTI spectra of Q2DW+2 and Q2DW+3 and scatter plot them against the corresponding MSMR amplitudes in Figures 3e and 3f, respectively. Overall, the MIGHTI Q2DW+2 is stronger than the MSMR amplitudes. The former attains  $20\text{--}25 \text{ ms}^{-1}$  whereas the latter is below  $15 \text{ ms}^{-1}$ . In the case of Q2DW+3, MIGHTI results exhibit excellent quantitative agreement with the MSMR results, both of which attain  $30 \text{ ms}^{-1}$ .

The fitted amplitudes and phases for MIGHTI results above 96 km are shown in Figure 4 as a function of height at  $0^\circ$  and  $15^\circ\text{N}$  latitude. The profiles centered on  $-5^\circ$ ,  $+5^\circ$  and  $+25^\circ$  are not sufficiently different from neighboring profiles and therefore not shown here. Within DOY 15–23, the amplitudes maximize generally below 140 km where the profiles often possess two peaks. Also, the  $v$  maximum is about a factor of two smaller ( $\lesssim 10 \text{ ms}^{-1}$ ) for Q2DW+2 as compared with Q2DW+3 ( $\sim 20 \text{ ms}^{-1}$ ), whereas the  $u$  maximum for Q2DW+2 ( $12\text{--}14 \text{ ms}^{-1}$ ) is slightly larger than that for Q2DW+3. In addition, half the amplitude profiles show increases with altitude above a minimum near 140–150 km altitude, suggesting a source at higher altitudes. The profiles within DOY 41–49 share many of the same characteristics.

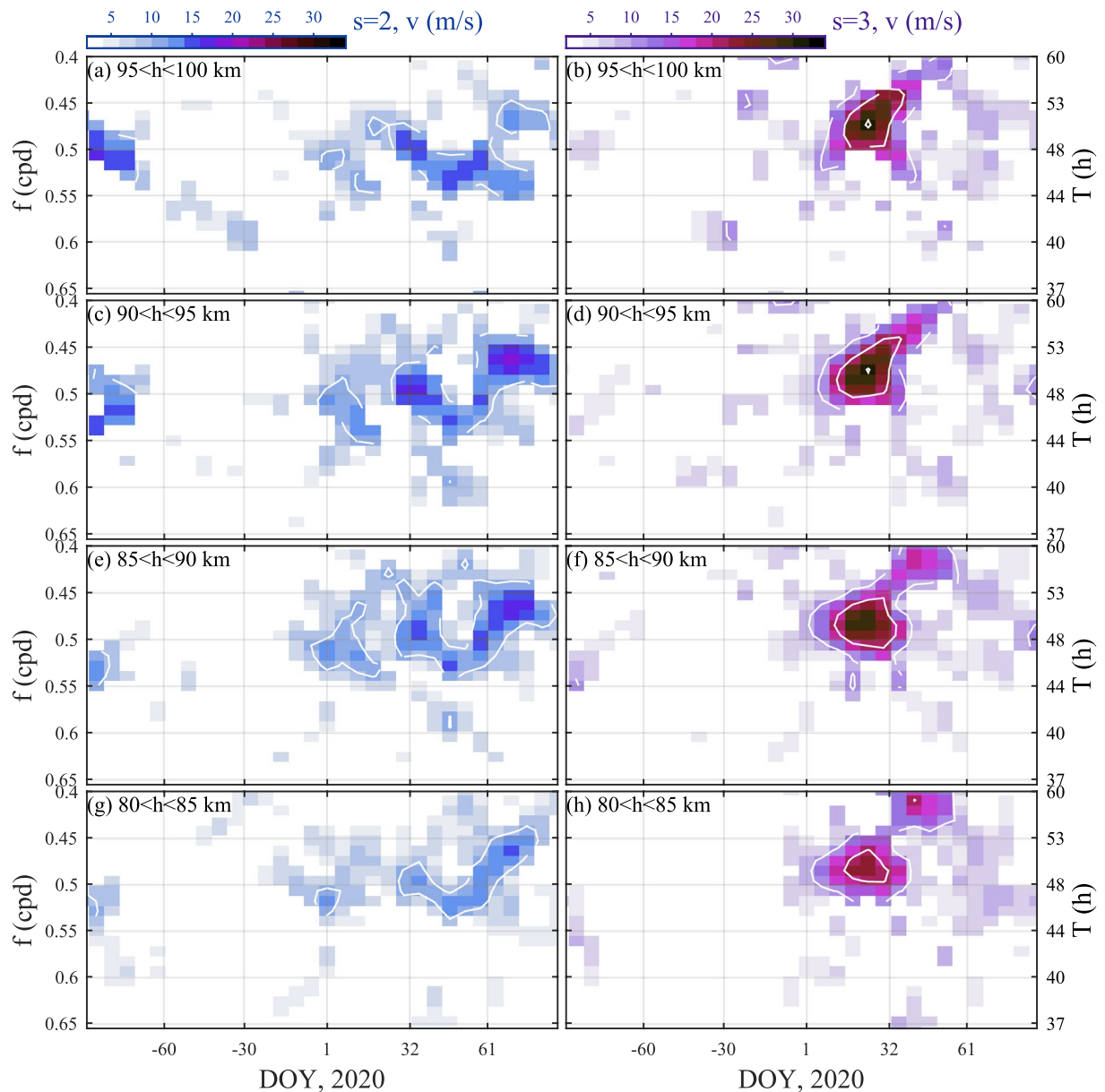


**Figure 1.** Amplitudes of quasi-2-day waves  $s = 2$  (left) and  $s = 3$  (right) in time-frequency depiction, in four altitude ranges estimated using the meridional winds from the four low-latitude radars. The white lines are contour lines of 10, 20, and 30  $\text{ms}^{-1}$ .

#### 4. Discussion

In the low-latitude middle atmosphere, Q2DWs maximize annually during late January and early February (Harris & Vincent, 1993; Palo & Avery, 1996). Harris and Vincent (1993) noted that the Q2DW-like oscillation in January–February 1991 occurs predominantly at a period 48–50 h, associated with a weaker one at 44 h. According to these periods the authors suggested that the oscillations are manifestations of Rossby-gravity modes Q2DW+3 and Q2DW+2, but could not determine  $s$  since they used single-station observations. Our multi-station analyses reveal that during January–February 2020 the most dominant Q2DWs are Q2DW+3 at 48–53 h and Q2DW+2 at 44–48 h. In addition, we find that: (a) the maximum Q2DW+3 amplitude is much stronger than the Q2DW+2 maximum, by a factor of about two, and (b) the Q2DW+3 are almost invariant within 80–100 km altitude, although slightly weaker at 80–85 km than at 85–100 km. Our analyses are the first to directly support the wavenumber suggestions of Harris and Vincent (1993).

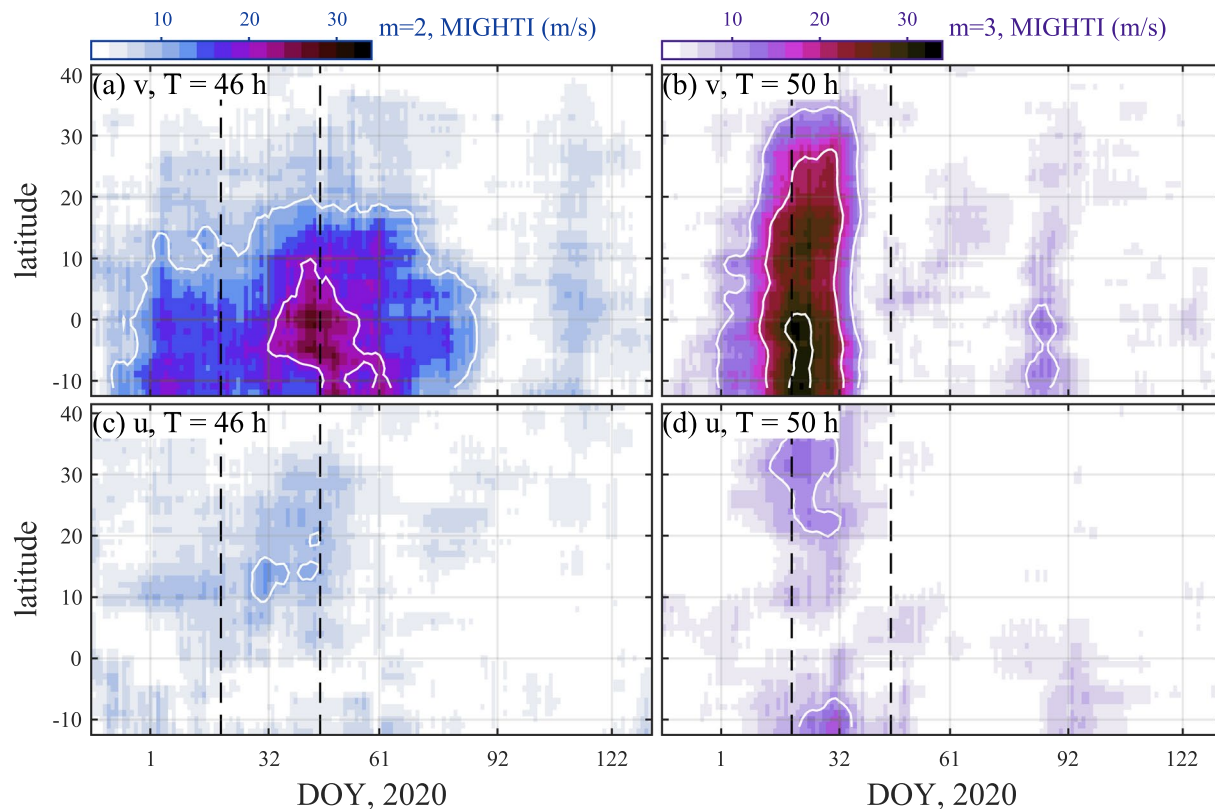


**Figure 2.** (a) Amplitudes of quasi-2-day waves with  $s = 2$  at 46-h period at 98 km altitude in time-latitude depiction estimated from Michelson Interferometer for Global High-resolution Thermospheric Imaging meridional wind. (b) same as (a) but for  $s = 3$  at 50-h period. (c) and (d) same as (a) and (b) but estimated from zonal winds. Vertical dashed lines indicate the centers of two 9 days windows used in Figure 4, which contain the maxima of the amplitudes and where daytime wind data are available above 106 km.

Note that our MSMR amplitudes are fitted according to the model of two waves with preassigned  $s$  which have to be determined prior to the fitting. Therefore, when the spectrum in the time-frequency depiction is dominated by a third  $s$ , the estimation cannot be properly fitted. For example, in Figure S3 besides  $s = +3$  and  $+2$ , the  $s = +1$  and  $+4$  dominate also a few pixels within DOY 1–60. For these pixels, the amplitudes are not fitted for Q2DW+1 and Q2DW+4 due to constraints of the two-wave model ( $r^2 < 0.7$ ). Besides, these four dominant Q2DWs might interact nonlinearly with diurnal migrating tides, generating SWs of Q2DW-3, Q2DW-2, Q2DW-1, and, Q2DW0. Additional low-latitude SMRs are desirable to resolve the above-mentioned Q2DWs.

In terms of the temporal evolution of Q2DW+3 amplitude and periods, MSMR results at 95–100 km are in excellent qualitative agreement with the MIGHTI results. The agreement reveals that locally Q2DW+3 is dominantly stronger than its potential aliased waves, for example, Q2DW-2, near-16-h and -9.6-h SWs, and near-2-days UFKW at  $s = -2$ , as explained in the introduction. Therefore MSMR help to resolve this type of ambiguity in MIGHTI Q2DW results. However, Q2DW+2 are stronger in the MIGHTI winds than in MSMR winds. The discrepancy is possibly attributable to a superposition in the MIGHTI amplitude between Q2DW+2 and its potential aliased waves, for example, Q2DW-1.

At altitudes not covered by MSMRs, for example, above 106 km, aliasing and superposition might also exist. The superposition could produce the vertical double-peak feature below 140 km altitude observed in Figure 4, associated in some cases with discontinuities, which would be unexpected for a vertically propagating monochromatic wave. The phases often show downward (upward) phase progressions with altitude, indicative of upward (downward) energy propagation. MLT GCM simulations produced near-48-h, -16-h, -9.6-h SWs arising from interactions of Q2DW+3 with diurnal and semidiurnal migrating tides (Gu et al., 2018; Nguyen et al., 2016; Palo et al., 1999). These SWs appear in the simulations as independent,

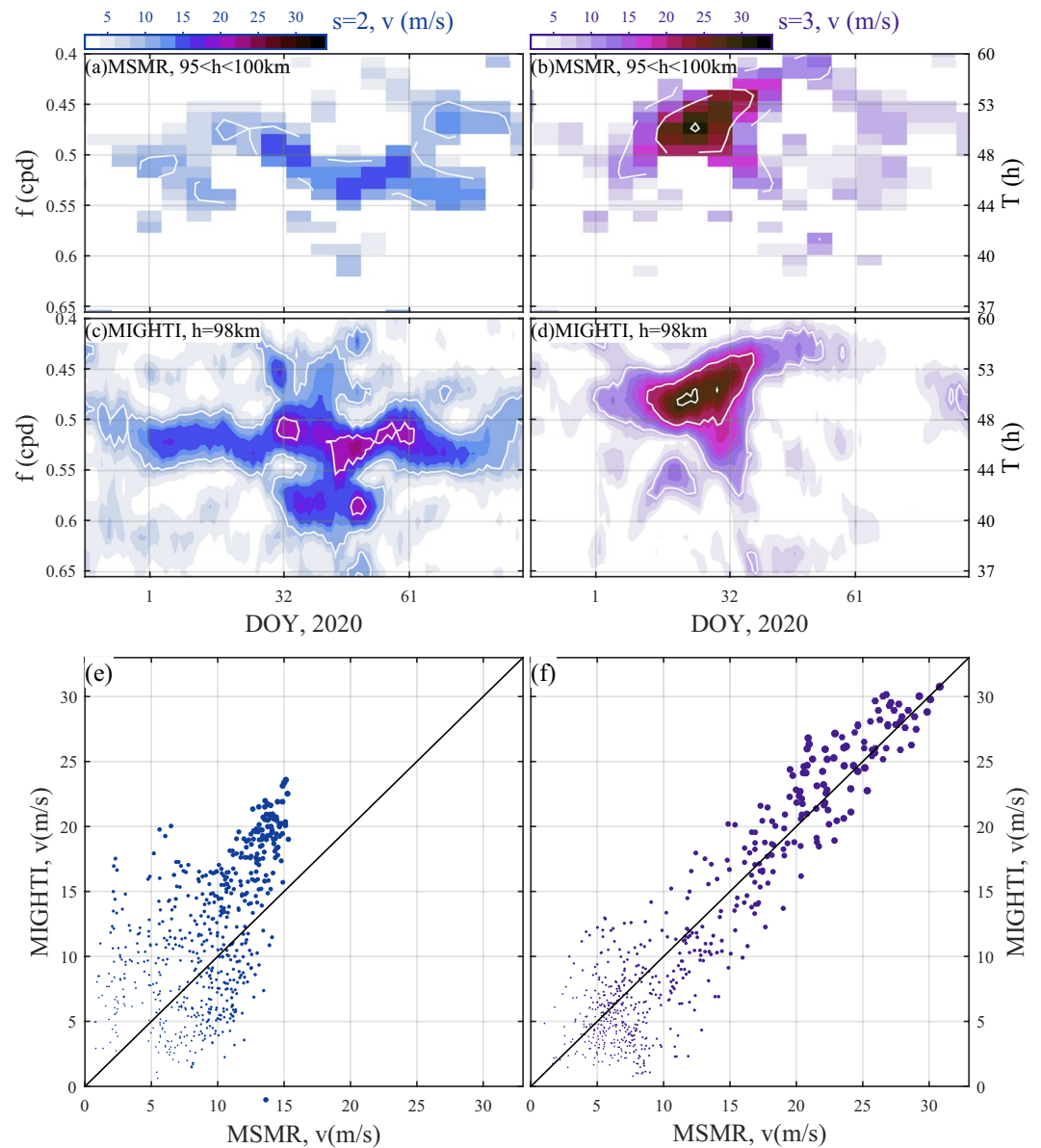


**Figure 3.** Meridional wind quasi-2-day waves amplitude comparisons between multiple SMR (MSMR) and Michelson Interferometer for Global High-resolution Thermospheric Imaging (MIGHTI) results. (a), and (b) MSMR results between 95 and 100 km for  $s = 2$  and  $s = 3$  component. (c) and (d) same plots as (a), and (b) but estimated from MIGHTI winds at 98 km altitude. (e) scatter plot of the values sampled from (a) and (c), in which each point denotes one pixel in (c) and its size is weighted by the sum of the amplitudes squared. (f) same plots as (e) but sampled from (b) and (d).

global-scale vertically propagating oscillations that extend to at least 50°N in January. Moreover, the simulations demonstrate that these SWs are capable of propagating into the 100–140 km region, and in some cases, above 160 km. It is, therefore, reasonable to assume that during Q2DW events, measurable SWs can simultaneously occur over broad latitude-altitude regimes, and that more appropriate designations in the context of space-based observations are “apparent” Q2DW+2, Q2DW+3, and Q2DW+4.

The presence of the SWs in the middle thermosphere is traditionally explained in terms of upward propagation of SWs generated in the MLT (see e.g., Yue et al., 2016, Figure 6). No study to date has considered the possibility of SW in-situ generation in the lower and middle thermosphere (~100–250 km) where the migrating tidal winds exist due to thermal forcing by extreme ultraviolet solar radiation, and where

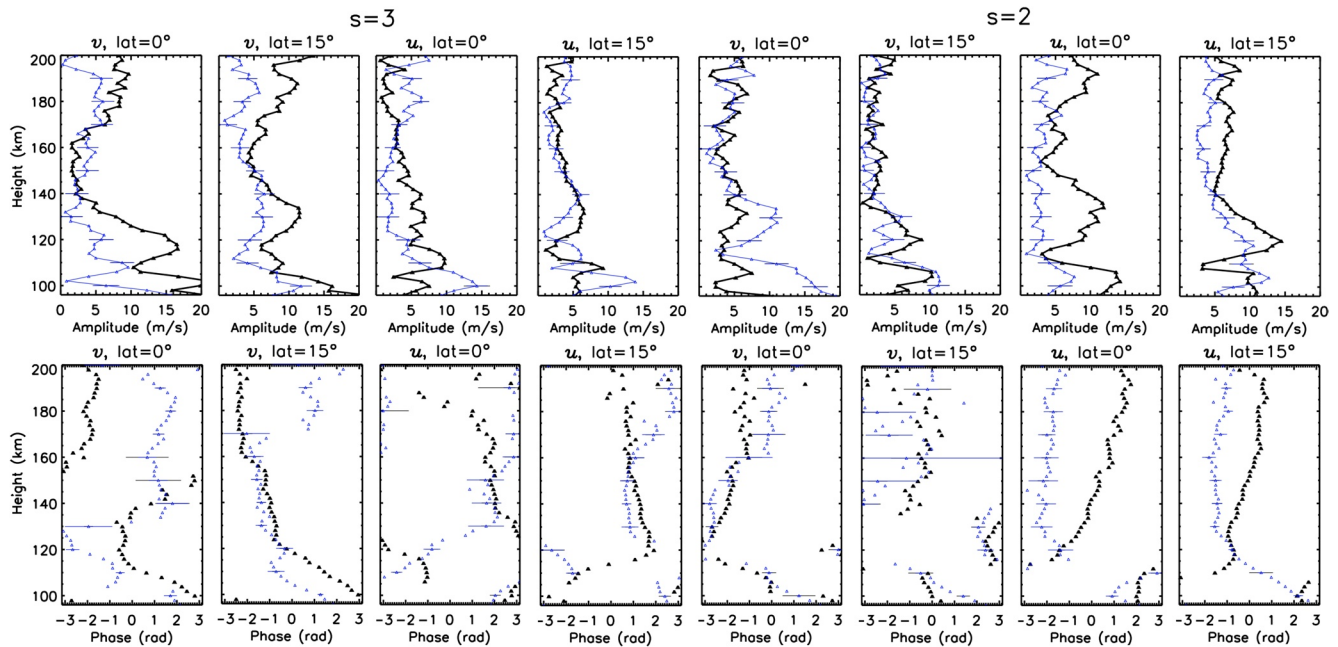


**Figure 4.** Vertical profiles of amplitude (top) and phase (bottom) for  $u$  and  $v$  centered on latitudes  $0^\circ$  and  $15^\circ$  for quasi-2-day waves with  $s = 3$  (left four columns) and  $s = 2$  (right four columns) for DOY 15–23 (black) and DOY 41–49 (blue).

the vertically propagating semidiurnal migrating tide maintains large amplitudes (e.g., Forbes, Zhang, & Maute, 2020, Figure 6). Palo et al. (1999) furthermore invoked the Teitelbaum and Vial (1991) formulation of wave-wave interactions to demonstrate that a myriad of wave products can originate from multi-step SW-tide interactions, including Q2DWs as secondary products. The multi-step SW-tide interaction process has been explained and demonstrated quantitatively in the context of thermospheric quasi-6-days waves by Forbes, Zhang, and Maute (2020). Our interpretation that these processes are likely active in defining the vertical amplitude and phase structures of Q2DW+3 and Q2DW+2 in Figure 4 warrants further theoretical and modeling attention.

A similar double-peak feature was also observed in the southern hemisphere Q2DW+3 in WINDII  $v$  profiles up to 150 km during January 19–31, 1993 (Ward et al., 1996). During this event, Q2DW+3 amplitudes and phases were estimated between 96–102 km and  $70^\circ\text{S}$ – $40^\circ\text{N}$  using WINDII, between 70–110 km and  $60^\circ\text{S}$ – $20^\circ\text{N}$  using the High Resolution Doppler Imager (HRDI) on UARS, and between 94–136 km altitude using winds collected by the Arecibo incoherent scatter radar ( $18^\circ\text{N}$ ) (Wu et al., 1993). Furthermore, the UARS analyses assumed  $T = 48$  h and  $s = 3$ .

In terms of Q2DW penetration into the winter hemisphere, the UARS results at 95–100 km are consistent with our Q2DW+3 results in that they (a) reflect an equatorial maximum in  $v$  with a monotonic decrease to less than half the maximum value by  $30^\circ\text{N}$ , and (b) a minimum in  $u$  at the equator and maximum as far north as  $30$ – $40^\circ$  latitude. However, both the  $u$  and  $v$  maxima are about a factor of 2 greater during 1993 than during 2020.

From a more global perspective, Ward et al. (1996) noted in their Figure 3 the similarity of the meridional 3-peaked (2-peaked) structure of  $u(v)$  between  $70^\circ\text{S}$ – $40^\circ\text{N}$  with those in the Q2DW+3 simulations of Hagan et al. (1993). Similar features are also seen in Palo et al. (1999) simulations, but the GCM  $u(v)$  structures in Yue, Wang et al. (2012) are more 2-peaked (1-peaked). All of these results maintain an equatorial minimum in  $u$  and a monotonic decrease in  $v$  poleward of the equator into the Northern Hemisphere. The tendency for an equatorial maximum in  $v$ , and maxima in  $u$  poleward of the equator is consistent with the attribution of Q2DW+3 as a Rossby-gravity wave. Therefore, the latitude structures of  $v$  and  $u$  for Q2DW+3 depicted in Figures 2a and 2c at 98 km are broadly consistent with prior observations, theory, and modeling.



Another unique aspect of the current work is the delineation of both Q2DW+3 and Q2DW+2 vertical structures up to 200 km altitude during a period of deep solar minimum, when vertically propagating waves should penetrate efficiently in the thermosphere (Häusler et al., 2013; Oberheide et al., 2009). Of particular relevance is the degree to which the Q2DW wind field penetrates to altitudes in the vicinity of the peak Hall (~106 km) and Pedersen (~125 km) conductivities, where electric fields can be generated and subsequently map into the F-region. This vertical penetration is in fact reflected in Figure 4, but it remains to be determined to what extent the amplitudes and vertical phase structures yield sufficiently large field-aligned-integrated conductivity-weighted winds to drive F-region ionospheric variability of any significance.

## 5. Summary and Conclusions

In this work, we combine MLT winds observed by four longitudinally separated low-latitude SMRs and by MIGHTI on the ICON satellite to investigate Q2DWs during January–March 2020. Based on different but complementary sensor array analyses, we identify that Q2DWs are dominated by Q2DW+3 and Q2DW+2, at periods  $T = 48$ –53 h and 44–48 h, respectively. These are the first observations of such waves and support the suggested Q2DW wavenumbers of Harris and Vincent (1993) based on single-station observations.

Our MSMR Q2DW amplitudes are almost altitude-independent within 80–100 km. Their 95–100 km time-frequency structures compared well with the amplitudes estimated from MIGHTI winds. In the comparison, Q2DW+3 exhibits an excellent quantitative agreement whereas the Q2DW+2 exhibits only a reasonable qualitative agreement with stronger amplitudes in MIGHTI than in MSMR results. Based on this agreement, we are able to resolve the period and wavenumber ambiguity in MIGHTI estimates. We attribute the discrepancy to the existence of aliased waves.

The MIGHTI measurements are further used to assess the latitudinal and vertical penetration of the Q2DWs, up to 42°N and 200 km. At 98 km and for both Q2DW+2 and Q2DW+3, the amplitudes in  $v$  are stronger than in  $u$ . For Q2DW+3, these features are largely consistent with prior observations, theory and modeling, whereas for Q2DW+2 the height-latitude structures have not appeared in prior observational or modeling studies. Above 106 km, the amplitudes become vertically structured. These vertical structures are attributable to the superposition between Q2DWs and their aliased waves.

## Data Availability Statement

The hourly wind data from Ledong is provided by the Data Center for Geophysics, National Earth System Science Data Sharing Infrastructure at BNOSE, IGGCAS (<http://wdc.geophys.ac.cn/>). The post-processed MSMR data used in the current paper are available at <https://dx.doi.org/10.22000/421>. The ICON-MIGHTI winds are publicly available at the ICON data center (<https://icon.ssl.berkeley.edu/Data>).

## Acknowledgments

This work was supported by the Deutsche Forschungsgemeinschaft (DFG, German Research Foundation) under SPP 1788 (DynamicEarth)-CH 1482/1–2 (DYNAMITE). C. Englert, J. Forbes, B. Harding, T. Immel, J. Makela, J. Harlander, K. Marr, and X. Zhang gratefully acknowledge support for this project by the ICON mission, which is supported by NASA's Explorers Program through contracts NNG12FA45C and NNG12FA42I. G. Li acknowledges the support of NSFC (42020104002, 41727803).

## References

- Chau, J. L., Urco, J. M., Vierinen, J., Harding, B. J., Clahsen, M., Pfeiffer, N., et al. (2021). Multistatic specular meteor radar network in Peru: System description and initial results. *Earth, Planets and Space*, 8(1), e2020EA001293. <https://doi.org/10.1029/2020EA001293>
- Chen, P.-R. (1992). Two-day oscillation of the equatorial ionization anomaly. *Journal of Geophysical Research*, 97(A5), 6343. <https://doi.org/10.1029/91ja02445>
- Englert, C. R., Harlander, J. M., Brown, C. M., Marr, K. D., Miller, I. J., Stump, J. E., et al. (2017). Michelson interferometer for global high-resolution thermospheric imaging (MIGHTI): Instrument design and calibration. *Space Science Reviews*, 212(1–2), 553–584. <https://doi.org/10.1007/s11214-017-0358-4>
- Forbes, J. M., He, M., Maute, A., & Zhang, X. (2020). Ultrafast Kelvin wave variations in the surface magnetic field. *Journal of Geophysical Research: Space Physics*, 125(9), e2020JA028488. <https://doi.org/10.1029/2020JA028488>
- Forbes, J. M., & Moulden, Y. (2012). Quasi-two-day wave-tide interactions as revealed in satellite observations. *Journal of Geophysical Research*, 117(12), D12110. <https://doi.org/10.1029/2011JD017114>
- Forbes, J. M., Zhang, X., & Maute, A. (2020). Planetary wave (PW) generation in the thermosphere driven by the PW-modulated tidal spectrum. *Journal of Geophysical Research: Space Physics*, 125(5), 1–19. <https://doi.org/10.1029/2019JA027704>
- Gu, S. Y., Li, T., Dou, X., Wu, Q., Mlynczak, M. G., & Russell, J. M. (2013). Observations of quasi-two-day wave by TIMED/SABER and TIMED/TIDI. *Journal of Geophysical Research: Atmospheres*, 118(4), 1624–1639. <https://doi.org/10.1002/jgrd.50191>
- Gu, S. Y., Liu, H. L., Dou, X., & Jia, M. (2018). Ionospheric variability due to tides and quasi-two day wave interactions. *Journal of Geophysical Research: Space Physics*, 123(2), 1554–1565. <https://doi.org/10.1002/2017JA025105>
- Hagan, M. E., Forbes, J. M., & Vial, F. (1993). Numerical investigation of the propagation of the quasi-two-day wave into the lower thermosphere. *Journal of Geophysical Research*, 98(D12), 23193–23205. <https://doi.org/10.1029/93jd02779>

- Harding, B. J., Chau, J. L., He, M., Englert, C. R., Harlander, J. M., Marr, K. D., et al. (2021). Validation of ICON-MIGHTI thermospheric wind observations: 2. Green-line comparisons to specular meteor radars. *Journal of Geophysical Research: Space Physics*, 126, e2020JA028947. <https://doi.org/10.1029/2020JA028947>
- Harding, B. J., Makela, J. J., Englert, C. R., Marr, K. D., Harlander, J. M., England, S. L., & Immel, T. J. (2017). The MIGHTI wind retrieval algorithm: Description and verification. *Space Science Reviews*, 212(1–2), 585–600. <https://doi.org/10.1007/s11214-017-0359-3>
- Harris, T. J., & Vincent, R. A. (1993). The quasi-two-day wave observed in the equatorial middle atmosphere. *Journal of Geophysical Research*, 98(D6), 10481. <https://doi.org/10.1029/93jd00380>
- Häusler, K., Oberheide, J., Lühr, H., & Koppmann, R. (2013). The geospace response to nonmigrating tides. In *Climate weather sun-earth system* (pp. 481–506). Springer.
- He, M., & Chau, J. L. (2019). Mesospheric semidiurnal tides and near-12 h waves through jointly analyzing observations of five specular meteor radars from three longitudinal sectors at boreal midlatitudes. *Atmospheric Chemistry and Physics*, 19(9), 5993–6006. <https://doi.org/10.5194/acp-19-5993-2019>
- He, M., Chau, J. L., Stober, G., Li, G., Ning, B., & Hoffmann, P. (2018). Relations between semidiurnal tidal variants through diagnosing the zonal wavenumber using a phase differencing technique based on two ground-based detectors. *Journal of Geophysical Research - D: Atmospheres*, 123(8), 4015–4026. <https://doi.org/10.1002/2018JD028400>
- He, M., Forbes, J. M., Chau, J. L., Li, G., Wan, W., & Korotyskin, D. V. (2020). High-order solar migrating tides quench at SSW onsets. *Geophysical Research Letters*, 47(6), 1–8. <https://doi.org/10.1029/2019GL086778>
- He, M., Forbes, J. M., Li, G., Jacobi, C., & Hoffmann, P. (2021). Mesospheric Q2DW interactions with four migrating tides at 53°N latitude: Zonal wavenumber identification through dual-station approaches. *Geophysical Research Letters*, 48, e2020GL092237. <https://doi.org/10.1029/2020GL092237>
- Huang, Y. Y., Zhang, S. D., Yi, F., Huang, C. M., Huang, K. M., Gan, Q., & Gong, Y. (2013). Global climatological variability of quasi-two-day waves revealed by TIMED/SABER observations. *Annales Geophysicae*, 31(6), 1061–1075. <https://doi.org/10.5194/angeo-31-1061-2013>
- Immel, T. J., England, S. L., Mende, S. B., Heelis, R. A., Englert, C. R., Edelstein, J., et al. (2018). The ionospheric connection explorer mission: Mission goals and design. *Space Science Reviews*, 214(1), 13. <https://doi.org/10.1007/s11214-017-0449-2>
- Ito, R., Kato, S., & Tsuda, T. (1986). Consideration of an ionospheric wind dynamo driven by a planetary wave with a two-day period. *Journal of Atmospheric and Terrestrial Physics*, 48(1), 1–13. [https://doi.org/10.1016/0021-9169\(86\)90108-X](https://doi.org/10.1016/0021-9169(86)90108-X)
- Lieberman, R. S. (1999). Eliassen-palm fluxes of the 2-day wave. *Journal of Atmospheric Science*, 56(16), 2846–2861. [https://doi.org/10.1175/1520-0469\(1999\)056<2846:EPFOTD>2.0.CO;2](https://doi.org/10.1175/1520-0469(1999)056<2846:EPFOTD>2.0.CO;2)
- Lima, L. M., Alves, E. O., Batista, P. P., Clemesha, B. R., Medeiros, A. F., & Buriti, R. A. (2012). Sudden stratospheric warming effects on the mesospheric tides and 2-day wave dynamics at 7°S. *Journal of Atmospheric and Solar-Terrestrial Physics*, 78–79, 99–107. <https://doi.org/10.1016/j.jastp.2011.02.013>
- Makela, J. J., Baughman, M., Navarro, L. A., Harding, B. J., Englert, C. R., Harlander, J. M., et al. (2021). Validation of ICON-MIGHTI thermospheric wind observations: 1. Nighttime red-line ground-based Fabry-perot interferometers. *Journal of Geophysical Research: Space Physics*, 126(2), 1–13. <https://doi.org/10.1029/2020ja028726>
- Meyer, C. K. (1999). Gravity wave interactions with mesospheric planetary waves: A mechanism for penetration into the thermosphere-ionosphere system. *Journal of Geophysical Research*, 104(A12), 28181–28196. <https://doi.org/10.1029/1999ja900346>
- Moudden, Y., & Forbes, J. M. (2014). Quasi-two-day wave structure, interannual variability, and tidal interactions during the 2002–2011 decade. *Journal of Geophysical Research*, 119(5), 2241–2260. <https://doi.org/10.1002/2013JD020563>
- Müller, H. G. (1972). A discussion on D and E region winds over Europe-long-period meteor wind oscillations. *Philosophical Transactions of the Royal Society A: Mathematical, Physical and Engineering Sciences*, 271, 585–599. <https://doi.org/10.1098/rsta.1972.0026>
- Nguyen, V. A., Palo, S. E., Lieberman, R. S., Forbes, J. M., Ortland, D. A., & Siskind, D. E. (2016). Generation of secondary waves arising from nonlinear interaction between the quasi 2 day wave and the migrating diurnal tide. *Journal of Geophysical Research - D: Atmospheres*, 121(13), 7762–7780. <https://doi.org/10.1002/2016JD024794>
- Oberheide, J., Forbes, J. M., Häusler, K., Wu, Q., & Bruinsma, S. L. (2009). Tropospheric tides from 80 to 400 km: Propagation, interannual variability, and solar cycle effects. *Journal of Geophysical Research - D: Atmospheres*, 114(23), 1–18. <https://doi.org/10.1029/2009JD012388>
- Palo, S. E., & Avery, S. K. (1996). Observations of the quasi-two-day wave in the middle and lower atmosphere over Christmas Island. *Journal of Geophysical Research*, 101(D8), 12833–12846. <https://doi.org/10.1029/96JD00699>
- Palo, S. E., Roble, R. G., & Hagan, M. E. (1999). Middle atmosphere effects of the quasi-two-day wave determined from a General Circulation Model. *Earth Planets and Space*, 51(7–8), 629–647. <https://doi.org/10.1186/BF03353221>
- Pancheva, D. (1988). Travelling quasi-two-day fluctuations in the summer F-region. *Comptes Rendus de l'Academie Bulgare des Sciences*, 41(11), 41–44.
- Pancheva, D., & Lysenko, I. (1988). Quasi-2-day fluctuations observed in the summer F region electron maximum. *Bulgarian Geophysical Journal*, 14(2), 41–51.
- Pancheva, D., Mukhtarov, P., & Siskind, D. E. (2018). Climatology of the quasi-2-day waves observed in the MLS/Aura measurements (2005–2014). *Journal of Atmospheric and Solar-Terrestrial Physics*, 171, 210–224. <https://doi.org/10.1016/j.jastp.2017.05.002>
- Pancheva, D., Mukhtarov, P., Siskind, D. E., & Smith, A. K. (2016). Global distribution and variability of quasi 2 day waves based on the NOGAPS-ALPHA reanalysis model. *Journal of Geophysical Research: Space Physics*, 121(11), 11422–11449. <https://doi.org/10.1002/2016JA023381>
- Pfister, L. (1985). Baroclinic instability of easterly jets with applications to the summer mesosphere. *Journal of the Atmospheric Sciences*, 42(4), 313–330. [https://doi.org/10.1175/1520-0469\(1985\)042<0313:BOEJW>2.0.CO;2](https://doi.org/10.1175/1520-0469(1985)042<0313:BOEJW>2.0.CO;2)
- Plumb, R. A. (1983). Baroclinic instability of the summer mesosphere: A mechanism for the quasi-two-day wave? *Journal of the Atmospheric Sciences*, 40(1), 262–270. [https://doi.org/10.1175/1520-0469\(1983\)040<0262:BIOTSM>2.0.CO;2](https://doi.org/10.1175/1520-0469(1983)040<0262:BIOTSM>2.0.CO;2)
- Randel, W. J. (1994). Observations of the 2-day wave in NMC stratospheric analyses. *Journal of the Atmospheric Sciences*, 51(2), 306–313. [https://doi.org/10.1175/1520-0469\(1994\)051<0306:OOTDWW>2.0.CO;2](https://doi.org/10.1175/1520-0469(1994)051<0306:OOTDWW>2.0.CO;2)
- Rao, N. V., Ratnam, M. V., Vedavathi, C., Tsuda, T., Murthy, B. V. K., Sathishkumar, S., et al. (2017). Seasonal, inter-annual and solar cycle variability of the quasi two day wave in the low-latitude mesosphere and lower thermosphere. *Journal of Atmospheric and Solar-Terrestrial Physics*, 152–153, 20–29. <https://doi.org/10.1016/j.jastp.2016.11.005>
- Rao, S. V. B., Eswaraiah, S., Venkat Ratnam, M., Kosalendra, E., Kishore Kumar, K., Sathish Kumar, S., et al. (2014). Advanced meteor radar installed at Tirupati: System details and comparison with different radars. *Journal of Geophysical Research*, 119(21), 11893–11904. <https://doi.org/10.1002/2014JD021781>
- Salby, M. L. (1981). Rossby normal modes in nonuniform background configurations. Part II: Equinox and solstice conditions. *Journal of the Atmospheric Sciences*, 38(9), 1827–1840. [https://doi.org/10.1175/1520-0469\(1981\)038<1827:RNMINB>2.0.CO;2](https://doi.org/10.1175/1520-0469(1981)038<1827:RNMINB>2.0.CO;2)

- Salby, M. L., & Roper, R. G. (1980). Long-period oscillations in the meteor region. *Journal of the Atmospheric Sciences*, 37(1), 237–244. [https://doi.org/10.1175/1520-0469\(1980\)037<0237:lpoitm>2.0.co;2](https://doi.org/10.1175/1520-0469(1980)037<0237:lpoitm>2.0.co;2)
- Teitelbaum, H., & Vial, F. (1991). On tidal variability induced by nonlinear interaction with planetary waves. *Journal of Geophysical Research*, 96(A8), 14169–14178. <https://doi.org/10.1029/91ja01019>
- Tunbridge, V. M., Sandford, D. J., & Mitchell, N. J. (2011). Zonal wave numbers of the summertime 2 day planetary wave observed in the mesosphere by EOS aura microwave limb sounder. *Journal of Geophysical Research*, 116(11), 1–16. <https://doi.org/10.1029/2010JD014567>
- Wang, Y., Li, G., Ning, B., Yang, S., Sun, W., & Yu, Y. (2019). All-sky interferometric meteor radar observations of zonal structure and drifts of low-latitude ionospheric E region irregularities. *Earth and Space Science*, 6(12), 2653–2662. <https://doi.org/10.1029/2019EA000884>
- Ward, W. E., Wang, D. Y., Solheim, B. H., & Shepherd, G. G. (1996). Observations of the two-day wave in WINDII data during January, 1993. *Geophysical Research Letters*, 23(21), 2923–2926. <https://doi.org/10.1029/96GL02897>
- Wu, D. L., Hays, P. B., Skinner, W. R., Marshall, A. R., Burrage, M. D., Lieberman, R. S., & Ortland, D. A. (1993). Observations of the quasi 2-day wave from the high resolution doppler imager on uars. *Geophysical Research Letters*, 20(24), 2853–2856. <https://doi.org/10.1029/93GL03008>
- Yue, J., Liu, H. L., & Chang, L. C. (2012). Numerical investigation of the quasi 2 day wave in the mesosphere and lower thermosphere. *Journal of Geophysical Research*, 117(5), D05111. <https://doi.org/10.1029/2011JD016574>
- Yue, J., Wang, W., Richmond, A. D., & Liu, H. L. (2012). Quasi-two-day wave coupling of the mesosphere and lower thermosphere-ionosphere in the TIME-GCM: Two-day oscillations in the ionosphere. *Journal of Geophysical Research: Space Physics*, 117(7), A07305. <https://doi.org/10.1029/2012JA017815>
- Yue, J., Wang, W., Ruan, H., Chang, L. C., & Lei, J. (2016). Impact of the interaction between the quasi-2 day wave and tides on the ionosphere and thermosphere. *Journal of Geophysical Research: Space Physics*, 121(4), 3555–3563. <https://doi.org/10.1002/2016JA022444>